The astrochemical factory: A solid base for interstellar reactions

Ligterink, N.F.W.

V-UV

$CO{:}CH_3OH(s) \rightarrow CO(g) + CH_3OH(g)$

$CH_3CHO(s)$

$CH_3OCH_3(s)$ $CH_3CH_2OH(s)$

$CH_3(s) + NCO(s) \rightarrow CH_3NCO(g)$

$CH_3 + NH_2CO \rightarrow CH_3CONH_2$

$CH_3NH_2(g)$

$CH_2NH + H \rightarrow CH_3NH_2$

$NO + H \rightarrow NH_2OH$

$H + Br \rightarrow HBr$

5

IR spectra of frozen complex organic molecules

J. Terwisscha van Scheltinga, N.F.W. Ligterink,
A.C.A. Boogert, E.F. van Dishoeck & H. Linnartz

Terwisscha van Scheltinga et al. 2017, *Infrared spectra of complex organic molecules in astronomically relevant ice matrices I: Acetaldehyde, ethanol and dimethyl ether*, subm. to A&A

5.1. Introduction

Water was the first molecule to be detected in the solid state in the interstellar medium (Gillett & Forrest 1973). Since then more than ten other molecules have been identified in icy form (i.e., CO, CO_2, CH_4, NH_3 and CH_3OH) and it has become clear that icy dust grains play a key role in the formation of both these small molecules and more complex organic molecules (COMs), like glycolaldehyde ($HOCH_2CHO$) and ethylene glycol ($HOCH_2CH_2OH$). The combined outcome of astronomical observations, specifically space based missions such as the *Infrared Space Observatory* (ISO) and *Spitzer Space Telescope* (Kessler et al. 1996; Werner et al. 2004), laboratory and astrochemical modelling studies have resulted in a detailed picture of the composition and structure of ice mantles on interstellar dust grains and the chemical processes taking place (see reviews by Gibb et al. 2000a; Herbst & van Dishoeck 2009; Öberg et al. 2011; Caselli & Ceccarelli 2012; Tielens 2013; Boogert et al. 2015; Linnartz et al. 2015; berg 2016). It is generally accepted that interstellar ices form on the surface of dust grains in cold dark clouds through accretion in two distinct layers, a polar H_2O-rich and an apolar CO-rich layer. Water, together with NH_3, CO_2 and CH_4, forms through atom addition reactions in lower density environments (Hiraoka et al. 1995; Miyauchi et al. 2008; Oba et al. 2009; Dulieu et al. 2010; Hidaka et al. 2011; Linnartz et al. 2011; Oba et al. 2012; Lamberts et al. 2013, 2014; Fedoseev et al. 2015b). At later stages, when densities increase and temperatures decrease along with the ongoing cloud collapse, CO freeze-out from the gas-phase occurs, forming a CO coating on top of the water rich layer (Tielens et al. 1991; Pontoppidan 2006). Subsequent hydrogenation processes transform CO to H_2CO and H_2CO to CH_3OH (Watanabe & Kouchi 2002; Fuchs et al. 2009), resulting in CO ice intimately mixed with methanol (Cuppen et al. 2011; Penteado et al. 2015). Radical recombination processes in different starting mixtures, triggered by energetic (i.e. UV photons or cosmic rays) or non-energetic (i.e. atom additions) were shown to provide pathways towards the formation of more complex molecules (see reviews of Linnartz et al. 2015; berg 2016).

The molecules H_2O, CO, CO_2, CH_4, NH_3 and CH_3OH make up the bulk of interstellar ice (Ehrenfreund & Charnley 2000; Öberg et al. 2011), but less abundant species have been observed as well. These include species such as OCS and OCN^- (Palumbo et al. 1995; van Broekhuizen et al. 2004). A number of COMs like formic acid (HCOOH), acetaldehyde (CH_3CHO) and ethanol (CH_3CH_2OH), have been tentatively detected based on spectroscopic features at 7.2 and 7.4 μm (Schutte et al. 1999; Öberg et al. 2011). Several other spectroscopic features, such as the 6.0 and 6.8 μm bands, remain only partly identified (Schutte et al. 1996; Boudin et al. 1998; Gibb & Whittet 2002; Boogert et al. 2008). Limited astronomical detection sensitivity combined with a lack of high resolution laboratory data have thus far prohibited secure solid state identifications of COMs other than methanol, but their presence in interstellar ices is generally accepted and also further supported by the recent detection of a number of COMs on comet 67P/Churyumov-Gerasimenko and in its coma (Goesmann et al. 2015; Altwegg et al. 2017).

With the upcoming launch of the *James Webb Space Telescope* (JWST) in 2018, new instruments such as MIRI (Mid InfraRed Instrument, Wright et al. 2015) and

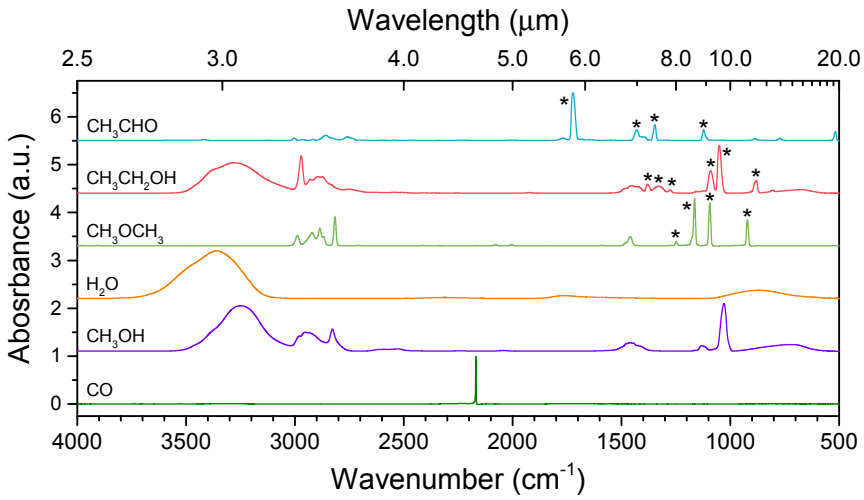

Figure 5.1: Spectra of pure acetaldehyde (blue), ethanol (red), dimethyl ether (green), water (orange) methanol (purple) and CO (dark green) normalised to one, in the range of 2.5 to 20.0 μm. The bands investigated in this work are indicated with an asterix (*).

NIRSpec (Near InfraRed Spectrograph) will become available to record telluric free spectra of interstellar ices at higher spectral and spatial resolution and with higher sensitivity than before. This opens up new possibilities to search for and study the level of molecular complexity in interstellar ices. To aid in the search for larger molecules in the solid state, high resolution IR laboratory spectra are required. The ice matrix environment and its temperature have to be taken into account, since these influence the spectral appearance of vibrational bands.

In this work we present the infrared spectra of acetaldehyde, ethanol and dimethyl ether, respectively, CH_3CHO, CH_3CH_2OH, and CH_3OCH_3. The choice for these three species is motivated by previous tentative identifications (Boudin et al. 1998; Schutte et al. 1999; Öberg et al. 2011), their astronomical gas-phase identification and high abundance (e.g. Turner 1991; Gibb et al. 2000a; Cazaux et al. 2003; Bisschop et al. 2007b; Taquet et al. 2015; Müller et al. 2016), and their common formation scheme upon UV irradiation of methanol ice (Öberg et al. 2009a). Formation of these molecules is seen in energetic processing experiments of methanol ice (Gerakines et al. 1996; Bennett et al. 2007; Öberg et al. 2009a; Boamah et al. 2014), and start with cleavage of the CH_3OH bonds. This results in a reservoir of radicals that can be used for their formation:

$^{\bullet}CH_3 + {}^{\bullet}CHO \rightarrow CH_3CHO$

$^{\bullet}CH_3 + {}^{\bullet}CH_2OH \rightarrow CH_3CH_2OH$

$^{\bullet}CH_3 + {}^{\bullet}OCH_3 \rightarrow CH_3OCH_3$

Formation of dimethyl ether and ethanol has also been studied by radical

Table 5.1: Selected bands of acetaldehyde, ethanol and dimethyl ether

Species		Formula	Mode	Peak position[a] cm^{-1}	Peak position[a] μm
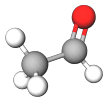	Acetaldehyde	CH_3CHO	C-C stretch	1122.3	8.909
			CH_3 s-deform.	1346.2	7.427
			CH_3 d-deform.	1429.4	6.995
			C=O stretch	1723.0	5.803
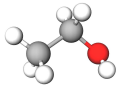	Ethanol	CH_3CH_2OH	C-C stretch	879.8	11.36
			C-O stretch	1051.0	9.514
			CH_3 rocking	1090.5	9.170
			CH_2 torsion	1275.2	7.842
			OH deform.	1330.2	7.518
			CH_3 s-deform.	1381.3	7.240
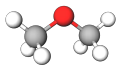	Dimethyl ether	CH_3OCH_3	C-O s-stretch	921.3	10.85
			C-O a-stretch	1093.9	9.141
			CH_3 rocking	1163.8	8.592
			CH_3 rocking	1248.2	8.011

Notes. [a]Peak position of the pure molecule at 15 K.

recombination reactions starting from CH_4:H_2O mixtures (Bergantini et al. 2017). Besides energetic radical recombination reactions, other formation pathways and links between the three molecules exist as well. For example, acetaldehyde has been proposed as a solid state precursor of ethanol. A hydrogen atom addition experiment showed that acetaldehyde can at least partially ($\geq$20%) be transformed into ethanol (Bisschop et al. 2007a). Acetaldehyde itself has been proposed to form as a spin-off in the well studied CO+H $\rightarrow$ HCO $\rightarrow$ H_2CO $\rightarrow$ H_3CO $\rightarrow$ CH_3OH chain (Charnley 2004). HCO may directly interact with a C-atom, to form HCCO that upon hydrogenation yields CH_3CHO (Charnley & Rodgers 2005).

This work presents a detailed study of the IR spectral characteristics of CH_3CHO, CH_3CH_2OH, and CH_3OCH_3 in pure form and mixed in the interstellar relevant ice matrices H_2O, CO, CH_3OH and CO:CH_3OH. Section 5.2 contains the experimental details and measurement protocols. The results of the measurements are presented and discussed in section 5.3. In section 5.4 the astronomical relevance of the new data is illustrated. The conclusions are summarized in Sect. 5.5. A complete overview with all data obtained in this study is available from the Appendices.

5.2. Experimental

5.2.1. Set-up

The ice spectra are recorded in a high-vacuum (HV) set-up which is described in detail by Bossa et al. (2015). A central stainless steel chamber is evacuated by a 300 $l\,s^{-1}$ turbomolecular pump, backed by a double stage rotary vane pump (8 $m^3\ hr^{-1}$). This allows a base pressure of $\sim 10^{-7}$ mbar at room temperature. The pressure is monitored by an Agilent FRG-720 full range gauge. Ices are grown on an infrared transmissive ZnSe window which is cryogenically cooled to a lowest temperature of 12 K by a closed cycle helium cryostat. The temperature of the window is monitored by a LakeShore 330 temperature controller, which regulates a feedback loop between a resistive heating wire and a silicon diode temperature sensor. An absolute temperature accuracy of ± 2 K and a relative accuracy of ± 1 K is acquired with this diode. The IR beam of a Fourier Transform InfraRed Spectrometer (FTIRS, Varian 670-IR) is aligned through the window in order to obtain IR spectra of the samples. The spectrometer covers a range of 4000 to 500 cm^{-1} (2.5–20 μm) at spectral resolutions as high as 0.1 cm^{-1}. Pure or premixed gases are background deposited onto the sample via an inlet valve. Samples are externally prepared in a gas mixing system. The gas mixing line is turbomolecularly pumped to pressures ¡ 1×10^{-4} mbar. Two gas independent gauges, covering different pressure ranges ensure that accurate mixing ratios are obtained. The liquids and gases used in these experiments are: acetaldehyde (Sigma-Aldrich, 99.5%), ethanol (Biosolve, 99.9%), dimethyl ether (Sigma-Aldrich, 99.9%), water (Milli-Q, Type I), carbon monoxide (Linde gas, 99.997%), and methanol (Sigma-Aldrich, 99.9%). Liquid samples are purified with freeze-pump-thaw cycles before use.

5.2.2. Measurement protocol

A 2L glass bulb is filled on the gas mixing system with a pure or mixed gas sample to a standard pressure of 20 mbar. This is a large enough gas reservoir to prevent a decreasing inlet pressure gradient during deposition. Bi-mixed gases are prepared in a 1:20 ratio and tri-mixed gases in a 1:20:20 ratio, where the smallest fraction is the COM under investigation. These dilution factors ensure that the COM mainly interacts with the surrounding matrix, resulting in matrix shifted IR vibrational bands. Ices are grown at 15 K to a thickness of $\sim$4500 ML (1 ML = 1×10^{15} molecules cm^{-2}) on the window. This thickness ensures that any influence of background contamination, mainly water depositing at a rate of less than 30 ML hr^{-1}, can be neglected. During deposition, IR spectra are recorded at 1 cm^{-1} resolution (0.5 cm^{-1} step size) and averaged over 61 scans (equals 2 minutes) to trace the ice growth and determine when the ice is $\sim$4500 ML thick. From the integration of the IR band absorption, the column density of the species N_{species} is determined according to:

$$N_{\text{species}} = \ln(10)\frac{\int_{\text{band}} \tau d\nu}{A_{\text{band}}}, \tag{5.1}$$

where $\int_{\text{band}} \tau d\nu$ is the integrated absorbance of the band and A_{band} the band strength in cm molecule^{-1}. It is important to realize that strong absorbing bands may get saturated at high coverages, resulting in unreliable thickness measurements. In the experiments conducted, the CO band at 2135 cm^{-1} reaches saturation at high coverage, as do certain bands of pure acetaldehyde and dimethyl ether. For these species bands with a lower band strength can be used. An independent verification between the gas and ice mixture ratio is realized through solid state column density measurements using the IR spectra.

After deposition the sample is linearly heated at a rate of 25 K hr^{-1}, until it is fully desorbed from the window. The low temperature ramp ensures that the ice has sufficient time to undergo structural changes, particularly from the amorphous to the crystalline phase. During heating IR spectra are continuously recorded and averaged over 256 scans to trace spectral changes versus temperature.

5.2.3. Analysis protocol

Due to the very large amount of spectra that are recorded during the experiment, here only samples of representative IR spectra at temperatures where significant spectral changes occur are presented. These spectra are baseline subtracted and the peak position and band width at Full Width at Half Maximum (FWHM) are determined for selected spectral features. When the band of a COM is embedded in a spectral feature of a matrix molecule, also the matrix feature is subtracted when possible. In the case of peak splitting, the least intense peak is only taken into account when its peak position is clearly distinguishable. In a few cases splitted peaks rival in intensity and are heavily overlapping and it is not possible to fit a FWHM for the individual components. Here the FWHM of the combined peaks is determined. Peaks are selected for analysis mainly based on their intensity and potential as a molecule tracer, i.e., selecting wavelengths for which no strong overlap with known interstellar features exist. Identification of vibrational modes of the three species studied here is realized by comparison with available spectra from gas phase and solid state literature (Plyler 1952; Schneider & Bernstein 1956; Evans & Bernstein 1956; Taylor & Vidale 1956; Mikawa et al. 1971).

Optical effects like Longitudinal Optical - Transverse Optical (LO-TO) splitting and particle shape effects are not explicitly taken into account. Since spectra are recorded at normal incidence with unpolarized light, only the TO modes are recorded. However, certain combinations of polarized light and angles of incidence can result in the LO phonon mode showing up (Baratta et al. 2000; Palumbo et al. 2006). Also particle shape effects can shift transition bands with respect to recorded laboratory spectra (Baratta & Palumbo 1998). Such effects will affect only the spectra of more abundant species, like CO or CO_2, and are not considered to be relevant for COMs.

5.3. Results and Discussion

In this section selected results of the acetaldehyde, ethanol and dimethyl ether experiments are presented. These are representative for the much larger

Table 5.2: Peak position and FWHM of the acetaldehyde CH_3 s-deformation mode at 15 K in various matrices.

Mixture	Temperature (K)	$\lambda_{peak,-baseline}$ (cm^{-1})	(μm)	$\lambda_{peak,-matrix}$ (cm^{-1})	(μm)	FWHM (cm^{-1})	(μm)
CH_3CHO	15	1346.6	7.4264	–	–	13.5	0.0744*
CH_3CHO :H_2O		1349.9	7.4078	1349.9	7.4078	9.2	0.0502
CH_3CHO :CO		1349.4	7.4104	–	–	4.8	0.0262
CH_3CHO :CH_3OH		1347.5	7.4211	–	–	13.0	0.0714
CH_3CHO :CO:CH_3OH		1349.4	7.4105	–	–	12.6	0.0691
CH_3CHO	30	1346.1	7.4290	–	–	13.7	0.0754
CH_3CHO :H_2O		1349.9	7.4078	1349.9	7.4078	8.8	0.0481
CH_3CHO :CO		1349.9	7.4078	–	–	6.1	0.0337*
CH_3CHO :CH_3OH		1347.5	7.4211	–	–	12.5	0.0686
CH_3CHO :CO:CH_3OH		1349.0	7.4131	–	–	12.2	0.0671
CH_3CHO	70	1346.1	7.4290	–	–	13.2	0.0729
CH_3CHO :H_2O		1349.4	7.4105	1349.4	7.4105	7.7	0.0420
CH_3CHO :CO		–	–	–	–	–	–
CH_3CHO :CH_3OH		1348.0	7.4184	–	–	10.9	0.0600
CH_3CHO :CO:CH_3OH		1348.5	7.4158	–	–	10.8	0.0592

*Notes.*Excerpt from Table B.1 in *AOP*. *FWHM result of two or more blended peaks.

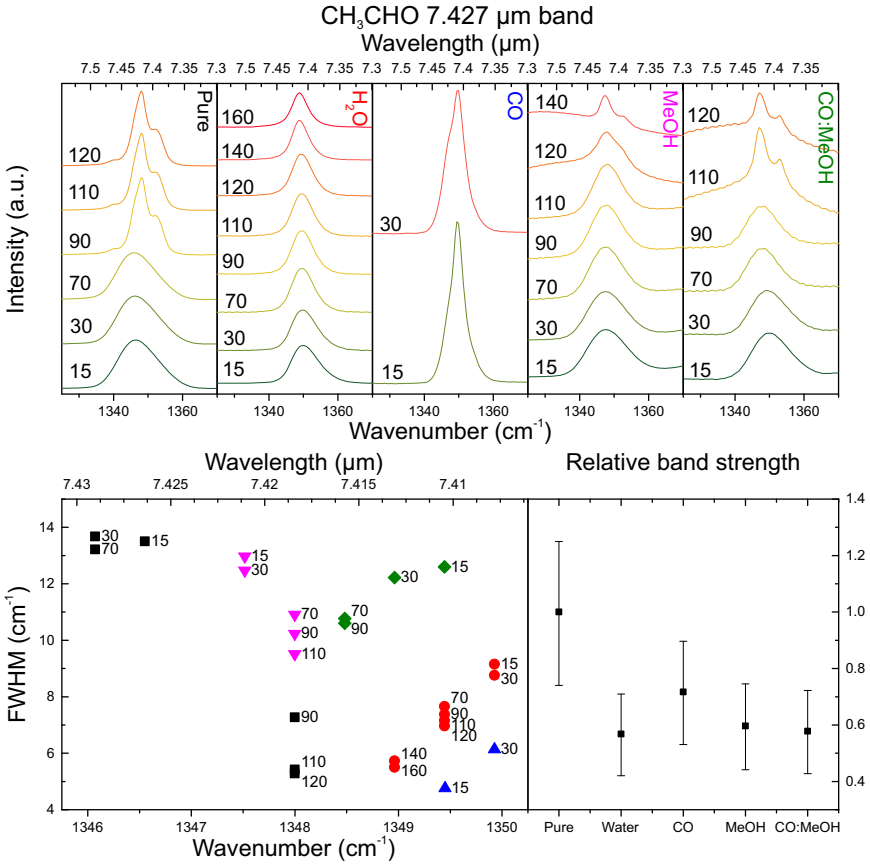

Figure 5.2: Top, from left to right the acetaldehyde 7.427 μm band pure (black) and in water (red), CO (blue), methanol (purple) and CO:CH_3OH (green) at various temperatures. Bottom left, peak position versus FWHM plot, using the same color coding. Bottom right, the relative band strength for the 7.427 μm band at 15 K in various matrices.

data set given in the Supplementary material. The extensive tables that contain information on peak positions and FWHM of the molecules investigated in this work can be found in the Appendix of the Original Publication, which is abbreviated to *AOP* throughout this chapter. All the baseline subtracted spectra used in this work are publicly available from the Leiden Database for Ice (http://icedb.strw.leidenuniv.nl). Figure 5.1 shows the IR spectra of pure acetaldehyde, ethanol and dimethyl ether ice at 15 K, with the bands that are fully analysed indicated with an asterix (*) and spectra of pure water, CO and methanol ice. Figures of the spectra of COMs mixed in water, CO, methanol and CO:methanol at 15 K are shown in Appendix A in the original publication. In Table 5.1 these selected bands are listed together with their peak positions in pure ices at 15 K. Appendix B in the original publication presents the results of the analysis of the selected bands, listing peak positions, FWHMs and integrated absorbance ratios at various temperatures and ice matrices. A representative example of the tables listed in the Appendix is shown in Table 5.2 for the

acetaldehyde CH_3 s-deformation mode at 15, 30 and 70 K.

For easier interpretation the results have been visualised in a number of plots, see Figs. 5.2, 5.3 and 5.4 for examples. Each plot covers the data of one band. The top part shows spectroscopic changes of the band under thermal processing in pure and mixed ices. The bottom left part plots peak position versus FWHM, showing trends in the band. The bottom right part gives an indication how the band strengths change relative from each other in various matrices. Assuming that the ice thickness is roughly the same for each experiment and that the gas mixing ratio represents the ice mixing ratio, the mixed ices are corrected for their dilution factor. The remaining figures of other bands can be found in Appendix C in the original publication.

A few general observations can be made. Most peaks display peak narrowing under thermal processing, which is due the ice changing to a crystalline phase. Mixed ice in CO and CO:CH_3OH can be exceptions, due to the volatility of CO and its removal from the ice at relatively low temperatures. Above 30 K, the desorption temperature of CO, these ices are often seen to display peak broadening.

Peak splitting, especially at high temperature is another effect that is generally seen. This can be caused by two or more modes contributing to a single feature at low temperature and becoming visible as the peaks begin to narrow at higher temperatures. Alternatively, the matrix can play a role and a peak is split due to different interactions of a functional group with its surroundings. For example, an ice can segregate under thermal processing and have part of the COM still intimately mixed with the matrix molecule, while another part is forming COMs cluster. Segregation is an effect most clearly seen in the COMs:CO ice mixtures.

Integrated absorbance ratios are given for the bands under investigation in each ice mixture. These ratios can provide a tool to estimate the likelihood of observing other bands upon detection of a specific transition. They can also be used as conversion factors to determine band strengths from known band strengths. The bands are normalised on the band with highest integrated absorbance at 15 K, unless this band is suspected to be in saturation or when the data set is incomplete over the investigated temperature range.

5.3.1. Acetaldehyde

Acetaldehyde hosts four significant features in the 5.5 - 12.5 μm region (see Fig. 5.1). Some smaller features are also visible, such as the C-C stretching mode close to 11 μm, however, its intensity is very small compared to the other bands. Two characteristic vibrational modes of acetaldehyde at 6.995 and 8.909 μm, coincide with methanol CH_3 rocking and deformation modes and are likely obscured in interstellar spectra. A solid state identification of acetaldehyde based on these vibrational modes is unlikely. The C=O stretching mode is the most prominent band in this spectrum. However, its location at 5.8 μm coincides with the C=O stretching mode of many other molecules, such as formaldehyde (H_2CO), formic acid (HCOOH) or formamide (NH_2CHO), that are expected to be present in interstellar ice, making it likely that this band is blended. The fourth band is the CH_3 s-deformation mode around 7.427 μm, which is found to have no substantial overlap with abundant bulk interstellar ice components and therefore

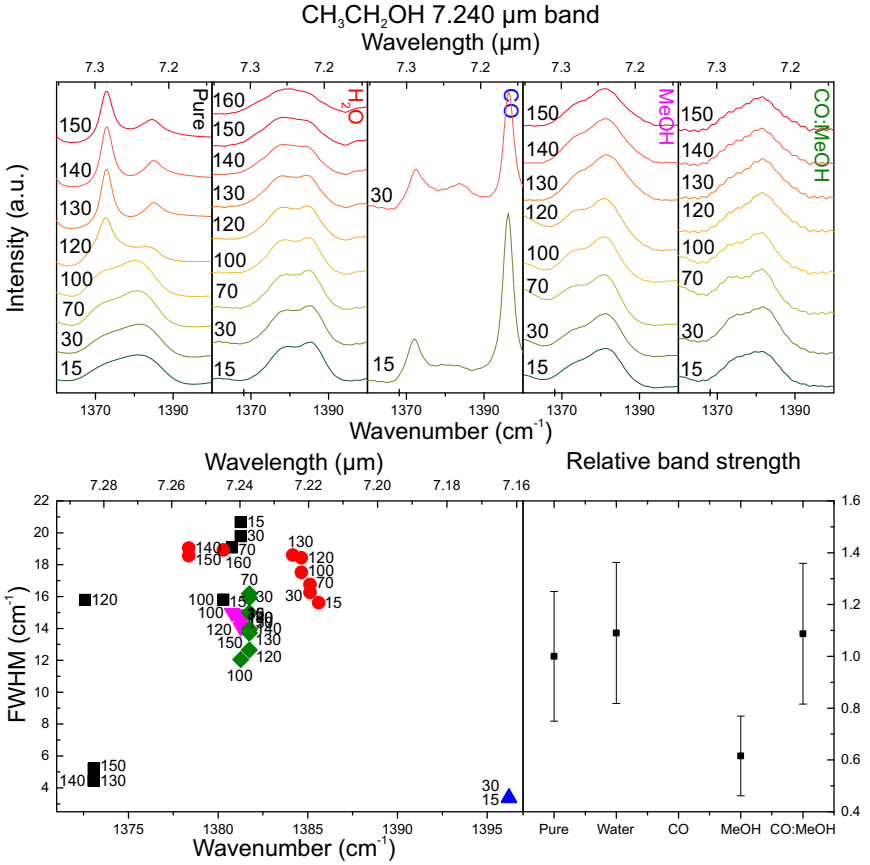

Figure 5.3: Top, from left to right the ethanol 7.842 μm band pure (black) and in water (red), CO (blue), methanol (purple) and CO:CH_3OH (green) at various temperatures. Bottom left, peak position versus FWHM plot, using the same color coding. Bottom right, the relative band strength for the 7.842 μm band at 15 K in various matrices.

is most suited for a successful solid state identification of this molecule.

Figure 5.2 shows the results of the analysed data of the CH_3 s-deformation band. Under thermal processing the band widths are generally seen to decrease, caused by crystallization in the ice. Peak positions shift as well, with clear blue shifting trends visible for the CO:CH_3OH and water mixtures. In the case of the CO:CH_3OH mixture this has likely to do with the loss of CO from the matrix, while for the water mixture the interaction between acetaldehyde and crystalline water is more likely the cause. In some cases, at high temperature CH_3CHO undergoes peak splitting, making identification through FWHM challenging. However, this can also be used as a tool to determine the ice temperature. The comparison of peak position makes it in general easy to distinguish between pure acetaldehyde, mixed in CO:CH_3OH and CH_3OH, mixed in CO and mixed in water. The 7.427 μm band shows a substantial decrease in band strength by about 40% when acetaldehyde is surrounded by matrix molecules.

The acetaldehyde C=O stretch band underlines the above findings, given it is

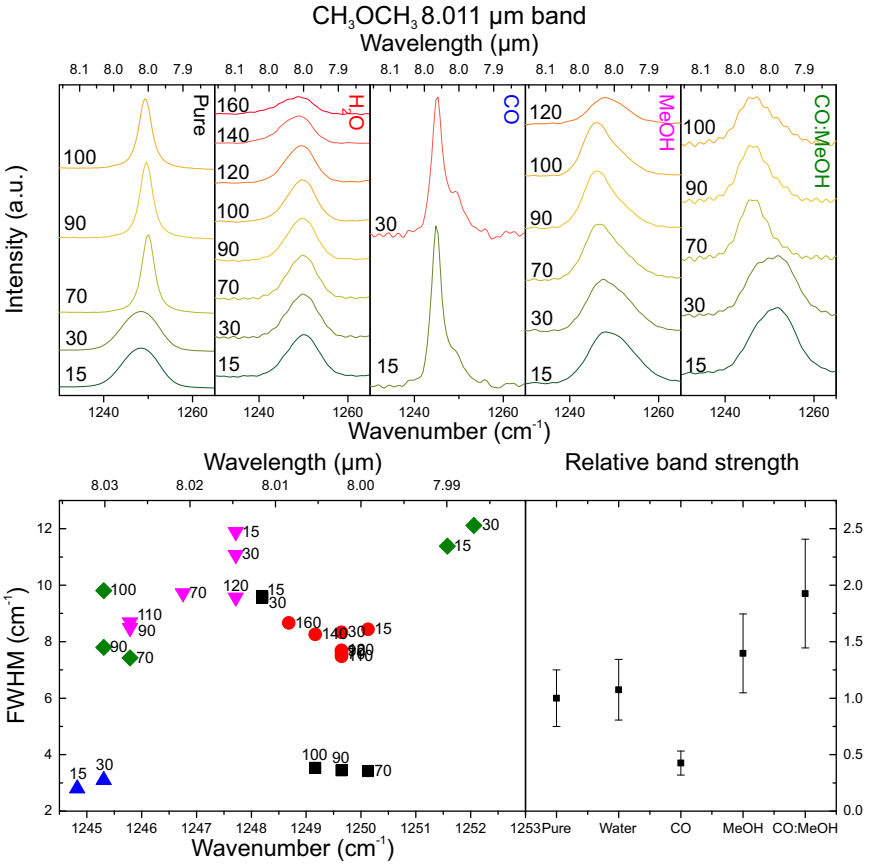

Figure 5.4: Top, from left to right the dimethyl ether 8.011 μm band pure (black) and in water (red), CO (blue), methanol (purple) and CO:CH_3OH (green) at various temperatures. Bottom left, peak position versus FWHM plot, using the same color coding. Bottom right, the relative band strength for the 8.011 μm band at 15 K in various matrices.

clearly observed (see Fig. C.3, *AOP*). Especially at low ice temperatures of 15 and 30 K clear peak shifts are visible between the CO:CH_3OH matrix at 5.84 μm, the water matrix at 5.825 μm and pure or in CH_3OH matrix at around 5.805 μm ices.

5.3.2. Ethanol

The spectrum of pure ethanol in Fig. 5.1 shows a strong C-C stretching band at 11.36 μm, C-O stretching mode at 9.514 μm and CH_3 rocking mode at 9.170 μm. A number of weaker modes are seen between 6.5 and 8.5 μm, specifically the CH_2 torsion mode at 7.842 micron, the OH deformation mode at 7.518 micron and the CH_3 symmetric deformation mode at 7.240 micron. Overlap with spectral features of bulk interstellar ice species like water and methanol is an issue for the three strongest bands, coinciding with either the water libration mode or C-O stretch and CH_3 rocking modes of methanol. Also the prominent broad silicate feature is present at $\sim$9.7 μm. Although the other ethanol modes are substantially weaker, they fall within a spectral region that is generally clean of strong transitions.

The ethanol 7.240 μm band is a likely candidate for identification. Figure 5.3 shows the data of this band. Ethanol mixed in water can be distinguished from other features by a $\sim$ 3 cm^{-1} peak shift from other mixtures. In general it is found that the ethanol:water mixture is relatively easy to distinguish, but the other mixtures display much overlap in peak position and FWHM. The CH_2 torsion, OH deformation mode and CH_3 symmetric deformation mode are hard to identify in the ethanol:CO mixture due to the appearance of many more modes. Band areas and relative band strengths of these modes are therefore not considered. The band strength is seen to vary substantially for the various bands, but does not show a clear trend.

5.3.3. Dimethyl ether

Three strong bands of dimethyl ether are found at 10.85, 9.141 and 8.592 μm for the C-O s-stretch, C-O a-stretch and CH_3 rocking mode, respectively. A much weaker CH_3 rocking mode is found at 8.011 μm. The first two overlap with known interstellar ice features of methanol, water and silicates and are therefore less suited for an identification, while the third likely falls in the wing of such features and may still be used. Despite being a weak mode, the 8.011 μm band does fall in a relatively empty region of interstellar ice spectra. This feature could therefore be most suited for an dimethyl ether identification, see Fig. 5.4.

For the 8.011 μm band clear differences are seen depending on the matrix. The spectra of pure and methanol mixture are distinguishable from those of the water and CO:CH_3OH mixtures by a $\sim$ 2 cm^{-1} peak shift of the low temperature spectra at 15 and 30 K. In water this band displays a narrower peak compared to the other ices. The other bands also show many clear differences in peak position and FWHM between the various ice mixtures. A characteristic peak splitting structure at low temperatures is seen for the 10.85 μm band when mixed in water, methanol or CO:CH_3OH. Interestingly the relative band strength shows a substantial increase in the CH_3OH and CO:CH_3OH mixtures for the 8.011 μm band. Other modes do not show such clear differences. Also interesting to note

is the fact that the C-O a-stretch has the largest band area when mixed in water, while in the other mixtures this is always the CH_3 rocking mode at 8.592 μm.

5.4. COM ice features in W33A

Our extensive measurements of frozen COMs will be needed in the analysis of the many spectra of dense clouds, embedded protostars, and inclined protoplanetary disks that will be obtained with the upcoming *JWST* mission at high sensitivity and medium spectral resolution (R of up to 3,000). Here, we demonstrate their use by a re-analysis of a spectrum of the massive protostar W 33A obtained with the Infrared Space Observatory's Short Wavelength Spectrometer (Astronomical Observation Template 1; R = 800). This is one of the few sources for which a high quality mid-IR spectrum is available (Gibb et al. 2000a). In the 7 to 8 μm region three prominent features at 7.25, 7.41 and 7.67 μm are described in the literature. The 7.25 μm feature has been attributed to both CH_3CH_2OH and HCOOH (Schutte et al. 1999; Öberg et al. 2011), the 7.41 μm feature has been attributed to $HCOO^-$ and CH_3CHO (Schutte et al. 1999) and the 7.67 μm band has been identified as solid methane with potentially contributions of SO_2 (Boogert et al. 1996).

In this work we make use of the water and silicate subtracted spectrum of W33A, shown in Fig. 5.5 with a straight line local continuum subtraction. The aforementioned features are visible, although the 7.41μm feature seems to have two contributions at 7.47 and 7.40 μm and the 7.25 μm feature is found at 7.22 μm. The spectra of ethanol and acetaldehyde mixed in CO:CH_3OH and H_2O are plotted in the same figure. The peak position of the 7.40 μm feature can be reproduced well by the acetaldehyde CH_3 s-deformation mode in both mixtures. However, the band in CO:methanol mixture seems to be too broad to justly reproduce the W33A 7.40 μm feature and also covers the 7.47 μm feature next to it. The other two features at 7.22 and 7.47 μm could be the result of the CH_3 s-deformation and OH deformation modes of ethanol. Particularly the CH_3CH_2OH:H_2O mixture coincides with the peak locations of the 7.22 and 7.47 μm features in the W33A spectrum. While the identification of acetaldehyde and ethanol are plausible, detection of additional features would strengthen the assignment. We checked and found that none of the other CH_3CHO and CH_3CH_2OH bands have an anticoincidence with the W33A spectrum.

Upper limits to the ice column densities of ethanol and acetaldehyde can be given based on the integrated optical depth of their potential features. Schutte et al. (1999) give integrated τ values of 2.0$\pm$0.3 and 1.6$\pm$0.5 cm^{-1}, respectively. Band strength values of ethanol and acetaldehyde are taken from the literature and used to calculate the column densities of the two features. The ethanol band strength of the C-O stretch mode at 9.514 μm has been determined in IR reflection experiments to be 7.3×10^{-18} cm molecule^{-1} (Moore & Hudson 1998). Since transmission bandstrengths for ethanol are not listed in the literature, we use this reflection value as an approximation. One has to be aware that experience learns that a mismatch by a factor of three can easily occur between tranmission and reflection bandstrengths. Using the integrated absorbance ratio CH_3 s-def. / C-O str. = 0.20 at 15 K from Table B.16 (*AOP*), the band strength of the CH_3 stretch mode is determined to be 1.5×10^{-18} cm molecule^{-1}. The effect of the

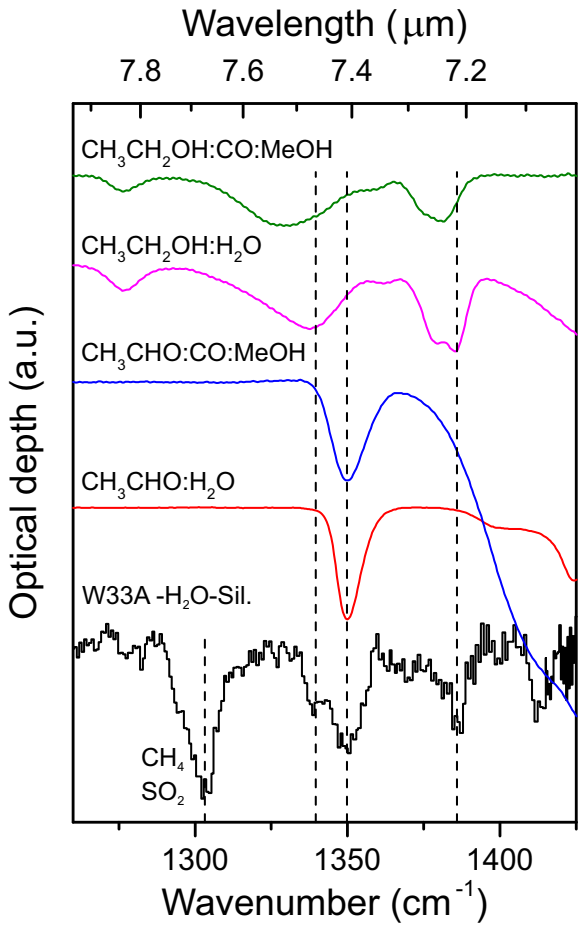

Figure 5.5: Continuum, water and silicate subtracted spectrum of W33A plotted together with ice spectra of ethanol and acetaldehyde at 15 K, mixed in :CO:CH_3OH and H_2O. Features in the W33A spectrum are indicated with dashed lines at 7.22, 7.40 and 7.47 micron. The large spectral feature at 7.67 μm is due to CH_4 and SO_2.

Table 5.3: Ice and gas-phase abundances of COMs toward W33A. Abundances given in %.

Species	Ice		Gas-phase[c]
	$/N(H_2O)$[a]	$/N(CH_3OH)$[b]	$/N(CH_3OH)$
CH_3CH_2OH	$\leq$3.4	$\leq$76	2.4
CH_3CHO	$\leq$2.3	$\leq$52	$\leq$0.2

Notes. [a]Keane et al. (2001); [b]Dartois et al. (1999); [c]Bisschop et al. (2007b)

matrix on the relative band strength is small for both the ethanol C-O stretch and CH_3 s-deformation modes, as can be seen from Figs. 5.3 and C.5 (*AOP*), and therefore assumed to be negligible. Assuming the entire 7.22 μm feature is caused by ethanol, this results in a column density of 1.3$\pm$0.2 $\times10^{18}$ cm^{-2}.

The acetaldehyde band strength is given as 1.3×10^{-17} for the C=O stretch mode (Wexler 1967). The integrated absorbance ratio of C=O str. / CH_3 s-deform. = 4.32 in pure acetaldehyde at 15 K in laboratory experiments, although the C=O stretch mode is likely saturated and the ratio may thus be higher. Using this ratio, the band strength of the CH_3 s-deformation mode is found to be 3.0×10^{-18} cm molecule^{-1}. As can be seen in Fig. 5.2, the relative band strength of this mode decreases substantially in mixtures by about 40%. The band strength of the CH_3 s-deformation mode in mixed ices is thus 1.8×10^{-18} cm molecule^{-1}. If the entire 7.40 μm feature is attributed to CH_3CHO, the resulting column density is 8.9$\pm$3 $\times10^{17}$ cm^{-2}.

In all likelihood the 7.22 and 7.40 μm features contain contributions of other molecules, mainly HCOOH and $HCOO^-$ and the reported values should therefore be seen as upper limits. Using solid water and methanol column densities of 3.8×10^{19} and 1.7×10^{18} cm^{-2}, respectively, toward W33A (Dartois et al. 1999; Keane et al. 2001), the upper limit abundance ratios of ethanol and acetaldehyde can be determined. $N(COM)/N(H_2O)$ are found to be $\leq$3.4% and $\leq$2.3%, while $N(COM)/N(CH_3OH)$ are $\leq$76% and $\leq$52% for ethanol and acetaldehyde, respectively. The abundances with respect to water are in good agreement with previously reported values of $\leq$4% and $\leq$3.6% for ethanol and acetaldehyde, respectively (Boudin et al. 1998; Schutte et al. 1999).

The $N(COM)/N(CH_3OH)$ upper limit ice abundance can be compared with known gas-phase abundances toward W33A. These are given as $N(CH_3CH_2OH)/N(CH_3OH)$ = 2.4% and $N(CH_3CHO)/N(CH_3OH) \leq$ 0.2% (Bisschop et al. 2007b) and are substantially lower than the ice upper limits. Interferometric observations with the Atacama Large Millimeter/submillimeter Array are needed to spatially resolve these molecules and determine more accurate abundances. Beside being upper limits, this difference may be linked to the process that transfers solid state species into the gas phase, causing molecules to fragment, or to destruction of species in the gas-phase. An overview of the COM abundances in ice and in the gas-phase toward W33A is given in Table 5.3.

The spectroscopic data presented in this chapter, combined with the improvements in terms of sensitivity and resolution of JWST will aid in confirming these detections and distinguish potential other contributors to these features. More observations, particularly towards low-mass sources, will give additional information about the carriers of these features.

5.5. Conclusions

This chapter adds to and extends on data of three important interstellar ice candidates, acetaldehyde, ethanol and dimethyl ether. A number of selected bands are fully characterized in FWHM and peak positions and show clear changes in various matrices. Our conclusions are summarized as follows:

1. The most promising bands to identify the COMs studied here in interstellar ice spectra are the 7.427 and 5.88 μm bands of acetaldehyde, the 7.240 and 11.36 μm bands of ethanol and the 8.011 and 8.592 μm bands of dimethyl ether.

2. Matrix characteristic shifts in peak position and FWHM are seen for several bands. The acetaldehyde CH_3 s-deform. and C=O stretch mode can be distinguished in H_2O, CO, CH_3OH and CO:CH_3OH matrices. Ethanol shows generally less distinctive shifts and only bands in the water matrix are unique. At low temperatures matrix specific dimethyl ether band shifts can be identified, specifically for the CH_3 rocking mode at 8.011 μm.

3. Given the higher complexity of the involved spectra, unambiguous identifications need to involve different bands that reflect bandwidths and intensity ratios as found in the laboratory studies. The dependence on matrix environment and temperature provides a tool to use these transitions as a remote diagnostic instrument.

4. Analysis of the ISO W33A spectrum in the 7 μm region shows a number of features that can be assigned to the COMs studied in this work. The 7.40 μm feature matches the position of the CH_3 s-deform. mode of acetaldehyde and the 7.22 μm feature is plausibly caused by the CH_3 s-deform. mode of ethanol. It is likely that 7.22 μm band is specifically caused by ethanol mixed in water. Abundances of both molecules with respect to water ice are determined to be $\leq$2.3% and $\leq$3.4% for acetaldehyde and ethanol, respectively.

Acknowledgement

I thank M.E. Palumbo for useful discussions on band profile changes due to grain shape differences and S. Ioppolo for many discussions.
This research was funded through a VICI grant of NWO, the Netherlands Organization for Scientific Research, Astrochemistry in Leiden is supported by the European Union A-ERC grant 291141 CHEMPLAN, by the Netherlands Research School for Astronomy (NOVA) and by a Royal Netherlands Academy of Arts and Sciences (KNAW) professor prize.